Supporting Information for:

Exploring the Binding Mechanism of Positive Allosteric Modulators in Human Metabotropic Glutamate Receptor 2 by Molecular Dynamics Simulations

Panpan Wang[†,*], Xiaonan Gao[†], Ke Zhang[‡], Qinglan Pei[†], Xiaobo Xu[†], Fengmei Yan[†], Jianghong Dong[†], Chenxi Jing[†]

[†] College of Chemistry and Pharmaceutical Engineering, Huanghuai University, Zhumadian 463000, China

[*] Corresponding Authors: Panpan Wang (wangpanpan@huanghuai.edu.cn)

TABLES

Table S1. All dissimilar coefficients for each PAMs pair in this work.

Drugs	ADX71149	AZD8529	BINA	JNJ40068782	JNJ46281222	JNJ42153605	JNJ46356479	THIIC
ADX71149	0	0.5805	0.6127	0.1215	0.5376	0.5367	0.5562	0.6276
AZD8529	0.5805	0	0.4747	0.5825	0.5108	0.5232	0.5254	0.3504
BINA	0.6127	0.4747	0	0.6149	0.7425	0.7490	0.7625	0.4856
JNJ40068782	0.1215	0.5825	0.6149	0	0.5233	0.5227	0.5424	0.6292
JNJ46281222	0.5376	0.5108	0.7425	0.5233	0	0.0377	0.0625	0.5175
JNJ42153605	0.5367	0.5232	0.7490	0.5227	0.0377	0	0.0614	0.5115
JNJ46356479	0.5562	0.5254	0.7625	0.5424	0.0625	0.0614	0	0.5192
THIIC	0.6276	0.3504	0.4856	0.6292	0.5175	0.5115	0.5192	0

Table S2. The calculated binding free energies of six systems on different windows (ΔG is in kcal/mol) during the whole 400 ns simulation[a].

Drugs	ADX71149	AZD8529	BINA	JNJ40068782	JNJ46281222	JNJ42153605	JNJ46356479	THIIC
50~100 ns	-53.59	-65.67	-63.68	-55.39	-60.27	-61.57	-51.7	-59.19
100~200 ns	-53.56	-66.18	-65.46	-55.4	-60.7	-60.72	-53.4	-59.82
200~300 ns	-53.58	-66.34	-67.5	-55.59	-60.74	-60.66	-52.98	-59.81
300~400 ns	-53.6	-66.15	-65.98	-55.56	-60.57	-60.7	-53.23	-60.74

[a] Calculated MM/GBSA binding free energies excluding the entropy contributions.

Table S3. The calculated and experimental binding energies of 8 studied PAMs binding to mGlu2 receptor (ΔG, $\Delta G'$ and $T\Delta S$ are in kcal/mol and K_i value is in nM).

Drugs	ΔE_{ele}	ΔE_{vdw}	ΔG_{pol}	ΔG_{nonpol}	$\Delta G'_{cacl(MM/GBSA)}$ [a]	$-T\Delta S$ [b]	$\Delta G_{cacl(MM/GBSA)}$ [c]	$\Delta\Delta G_{cacl(MM/GBSA)}$ [d]	K_i [e]	ΔG_{exp} [f]	$\Delta\Delta G_{exp}$
ADX71149	-6.47±0.07	-52.05±0.13	11.66±0.05	-6.74±0. 01	-53.60±0.13	13.88±0.21	-39.72±0. 34	7.06	180	-9.251	2.175
AZD8529	-7.77±0.11	-67.33±0.17	17.12±0.07	-8.17±0. 01	-66.15±0.16	27.66±0.69	-38.49±0. 85	8.29	371.54	-8.820	2.606
BINA	-110.97±0.38	-64.06±0.20	117.04±0.32	-7.99±0. 01	-65.98±0.17	25.11±0.36	-40.78±0.5 3	5.91	60.3	-9.903	1.523
JNJ40068782	-104.75±0.27	-54.78±0.15	110.72±0.24	-6.76±0. 01	-55.56±0.16	14.40±0.31	-41.16±0.4 7	5.62	26.3	-10.397	1.029
JNJ42153605	-14.29±0.07	-58.46±0.15	18.92±0.05	-6.74±0. 01	-60.57±0.16	17.07±0. 36	-43.5±0. 52	3.28	15	-10.732	0.694
JNJ46281222	65.31±0.18	-62.52±0.13	-55.96±0.16	-7.52±0. 01	-60.70±0.14	13.92±0.31	-46.78±0. 44	0	4.68	-11.426	0
JNJ46356479	71.94±0.24	-56.44±0.14	-61.77±0.22	-6.96±0. 01	-53.23±0.16	14.23±0.15	-39.00±0. 33	7.78	150	-9.360	2.066
THIIC	-119.4±0.32	-62.51±0.16	129.47±0.25	-8.3±0. 02	-60.74±0.19	19.69±0.24	-38.91±0. 43	7.87	79.43	-9.739	1.687

[a] Calculated binding energy in this work.

[b] Calculate interaction entropy ($-T\Delta S$) by normal mode analysis in this work.

[c] $\Delta G_{cacl(MM/GBSA)} = \Delta G'_{cacl(MM/GBSA)} + (-T\Delta S)$.

[d] $\Delta\Delta G_{cacl(MM/GBSA)} = \Delta G_{cacl(MM/GBSA)} - \Delta G_{JNJ46281222}$.

[e] Experimental K_i value from reported work in reference[1-4].

[f] Estimated binding energy based on K_i values using $\Delta G_{exp} = RT\ln(K_i), R = 8.314J/(K \cdot mol), T = 300K$.

Table S4. The components for relative binding free energy of PAMs with similarity from state A to B in $hmGlu_2$ via TI calculation (ΔG, ΔΔG are in kcal/mol, and K is in nmol).

Simulated transformation	Similarity score	transformation		Δ [a]	Δ [a]	Δ [a]	Δ [b]	ΔΔ [c]
JNJ46281222 →JNJ42153605	0.0378	4.68→15	Ligand	24.13	25.2	-118.75	-69.42	0.71
			Complex	24.39	25.38	-118.48	-68.71	
JNJ42153605 →JNJ46356479	0.0614	15→150	Ligand	118.66	-2.77	-167.7	-51.81	1.39
			Complex	119.15	-3.55	-166.02	-50.42	
ADX71149 →JNJ40068782	0.1215	180→26.3	Ligand	90.31	-1.25	-184.7	-95.64	-0.40
			Complex	90.57	-0.37	-186.24	-96.04	

[a] The energy calculated by thermodynamic integration based on λ ranging from 0.0 to 1.0

[b] ΔG is the sum of the ΔG_{ee}, ΔG_{e}, and ΔG_{ee}

[c] $\Delta\Delta G = \Delta G_{(\ )} \Delta G_{(i)}$

Table S5. The components for absolute binding free energy of 3 ligands with high dissimilarity in $hmGlu_2$ via TI calculation (ΔG is in kcal/mol, and K is in nmol).

PAMs		Δ	Δ	Δ	Δ [a]	Δ
AZD8529	371.54	-27.77±0.34	13.82±0.15	7.09	-0.41	-7.27±0.49
THIIC	79.43	-45.97±0.27	27.78±0.17	7.21	-0.41	-10.57±0.44
Bina	60.3	-43.05±0.41	23.97±0.29	6.7	-0.41	-12.77±0.70

[a] Δ = 2, $R = 8.314 J/(K \cdot mol)$, $T = 300K$

Table S6. Detailed energy terms calculated by the *in silico* single and multiple point(s) mutation analyses of this study in mGlu2 complexes (ΔG is in kcal/mol).

Mutation sites	Calculated values						Experimental values	
	ΔE_{ele}	ΔE_{vdw}	ΔG_{pol}	ΔG_{nonpol}	$\Delta\Delta G_{calc(MM/GBSA)}$ [a]	$FC_{calc(MM/GBSA)}$ [b]	FC_{exp} [c]	$\Delta\Delta G_{exp}$ [d]
F643A	61.67±0.16	-57.5±0.13	-54.46±0.13	-7.60±0 .01	2.8	109.99	79.37(26.31~239.76)	2.61(1.95~3.26)
S688L	61.44±0.15	-61.60±0.13	-52.74±0.11	-7.32±0. 01	0.46	2.16	3.39(2.00~5.75)	0.73(0.41~1.04)
G689V	61.77±0.13	-59.2±0.12	-54.41±0.11	-7.31±0. 01	1.54	13.27	10.23(3.02~34.66)	1.39(0.66~2.11)
L732A	62.5±0.16	-59.41±0.17	-55.59±0.14	-7.5±0. 01	0.71	3.29	8.12(2.24~29.50)	1.25(0.48~2.02)
N735D	40.23±0.28	-58.96±0.33	-32.6±0.23	-6.77±0. 02	2.59	77.31	35.46(12.31~102.28)	2.13(1.50~2.76)
W773A	63.15±0.16	-59.58±0.18	-55.55±0.22	-7.35±0. 01	1.37	9.97	12.87(7.59~21.86)	1.52(1.21~1.84)
S688L/G689V	63.61±0.29	-61.26±0.15	-54.25±0.26	-7.64±0. 01	1.15	6.89	11.74(2.69~51.26)	1.47(0.59~2.35)
S688L/G689V/N735D	64.74±0.29	-59.28±0.15	-56.03±0.23	-7.39±0. 01	2.73	97.79	69.13(21.88~218.66)	2.52(1.84~3.21)
S644A/V700L/H723V	67.33±0.28	-60.25±0.15	-58.69±0.24	-7.51±0. 01	1.58	14.19	13.17(4.47~38.88)	1.54(0.89~2.18)

[a] $\Delta\Delta G_{(MM/GBSA)} = \Delta G_{u\,i}\,\Delta G_{i\,ype}$.

[b] Fold-changes of potency ($_{(MM/GBSA)}$) were derived from $\Delta\Delta G_{(MM/GBSA)}$ the equation $\Delta\Delta G_{(MM/GBSA)} = RT\ln(_{(MM/GBSA)})$, $R = 8.314J/(K \cdot mol)$, $T = 300K$.

[c] Fold-changes of potency ($_{exp}$) measured by K_i values ($_{exp} = K_i(mutat\ on)/K_i(w\ ld\ type)$)[1, 5]. Numbers out of the bracket indicated the fold-changes derived from the mean experimental values of both $K_i(mutat\ on)$ and $K_i(w\ ld\ type)$. The first number in the bracket indicated the minimum fold-changes, while the second one indicated the maximum fold-changes.

[d] $\Delta\Delta G_{exp}$ were derived from the $_{exp}$ by the equation $\Delta\Delta G_{exp} = RT\ln(_{exp})$.

Table S7. Per-residue energy contributions of 23 residues shown in **Figure 4**.

Residue	ADX71149	AZD8529	BINA	JNJ40068782	JNJ42153605	JNJ46281222	JNJ46356479	THIIC
VAL613	-0.30	-0.17	-0.62	-0.58	-0.45	-0.40	-0.41	-0.61
CYS616	-0.69	-0.68	-0.75	-0.80	-0.69	-0.82	-0.76	-0.80
ARG636	0.00	-0.86	-4.97	-0.11	-0.01	-0.95	0.00	-0.52
LEU639	-1.96	-3.34	-2.69	-2.06	-2.34	-2.55	-1.16	-2.30
GLY640	-0.77	-0.59	-0.96	-0.46	-0.56	-0.66	-0.68	-0.47
ALA642	-0.38	-0.79	-0.70	-0.50	-0.33	-0.55	-0.24	-0.15
PHE643	-3.01	-1.82	-2.98	-3.12	-3.29	-4.33	-2.98	-3.59
CYS646	-0.55	-1.24	-0.49	-0.72	-0.44	-0.43	-0.32	-0.40
TYR647	-0.75	-1.70	-0.52	-0.71	-0.57	-0.63	-0.59	-0.90
MET728	-0.59	-1.08	-3.17	-0.63	-0.71	-2.11	-0.58	-2.48
SER731	-0.88	-0.35	-0.59	-0.67	-0.69	-0.88	-0.43	-1.05
LEU732	-1.74	-0.49	-0.76	-1.57	-1.99	-0.60	-1.44	-1.82
ASN735	-1.00	-0.30	-0.43	-0.79	-0.56	-0.16	-1.03	-0.48
ILE772	-0.76	-1.01	-0.20	-0.63	-0.59	-0.74	-0.67	-0.20
TRP773	-1.27	-2.97	-2.02	-1.47	-0.80	-0.82	-2.18	-0.61
PHE776	-0.39	-1.02	-0.42	-1.07	-1.14	-1.68	-1.82	-1.13
PHE780	-0.49	-2.41	-0.40	-0.44	-0.22	-0.12	-1.97	-0.89
MET794	-1.25	-1.27	-0.41	-1.24	-0.84	-1.40	-0.25	-1.02
SER797	-0.08	-0.50	-0.31	-1.77	-1.00	-1.20	-0.56	-1.44
VAL798	-1.80	-1.47	-2.10	-2.84	-2.33	-1.83	-1.49	-0.82
SER801	-0.59	-0.87	-0.90	-1.39	-1.17	-1.79	-1.47	-1.18
GLY802	-0.45	-0.29	-0.73	-0.47	-0.73	-0.53	-0.56	-0.40
VAL805	-0.44	-0.82	-0.48	-0.70	-0.25	-0.50	-0.63	-0.43

FIGURES

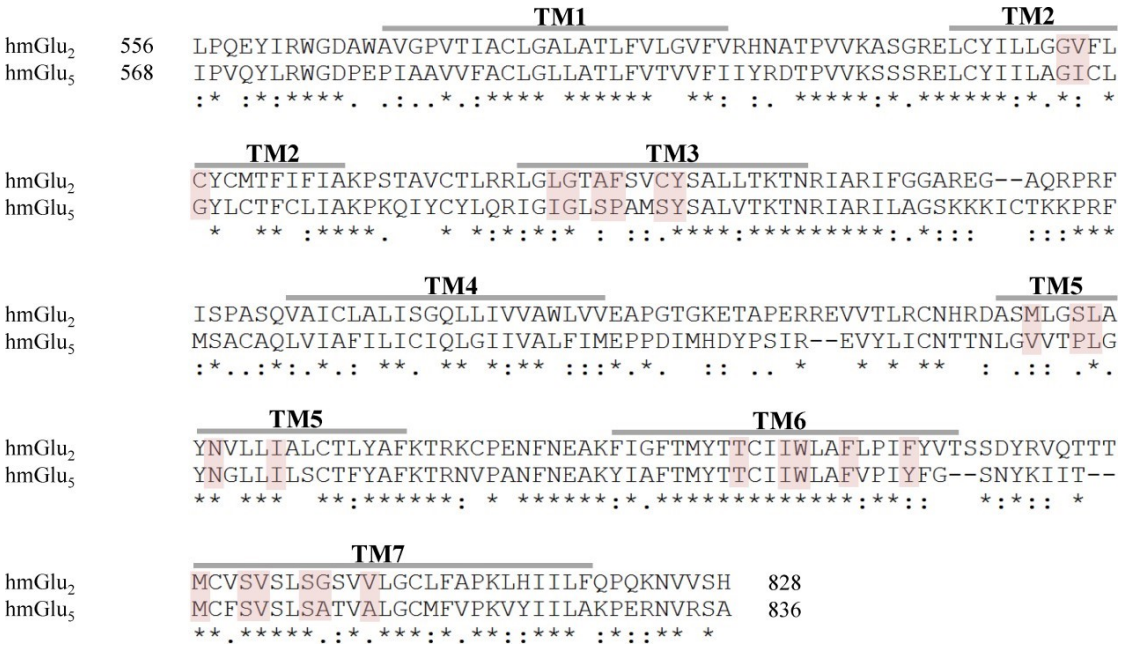

Figure S1. Sequence alignment between $hmGLu_2$ (from Leu556 to His828) and $hmGlu_5$ (from Ile568 to Ala836) using ClustalW2 program. The 7 transmembranes (TM1 to TM7) alpha helices were labeled above their sequence. Stars refer to the identical residues, the double filled periods refer to the conservative substitutions and the filled periods refer to the variable conservative substitutions. The comparison of allosteric sites between $hmGlu_2$ and $hmGlu_5$ receptors were illustrated by reddish solid rectangular.

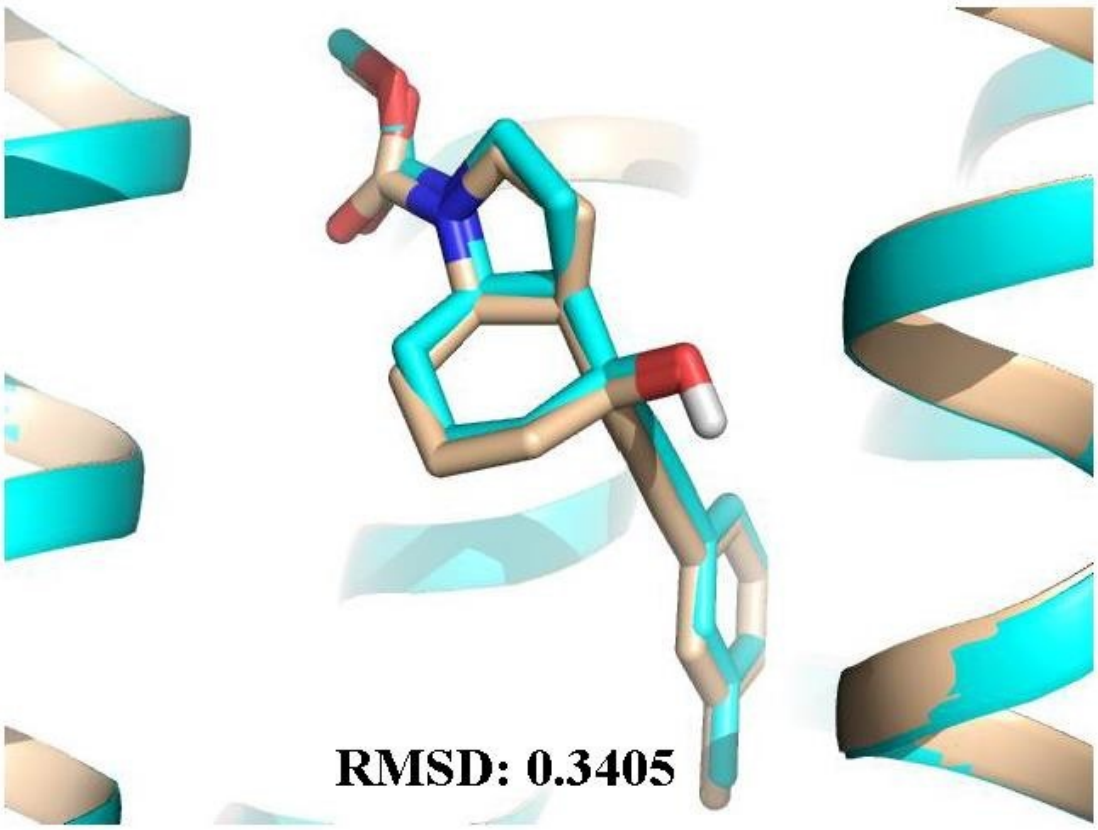

Figure S2. Structural superimposition of re-docking pose of Mavoglurant (cyan) with its co-crystallized pose (light brown) with 0.3405 of RMSD.

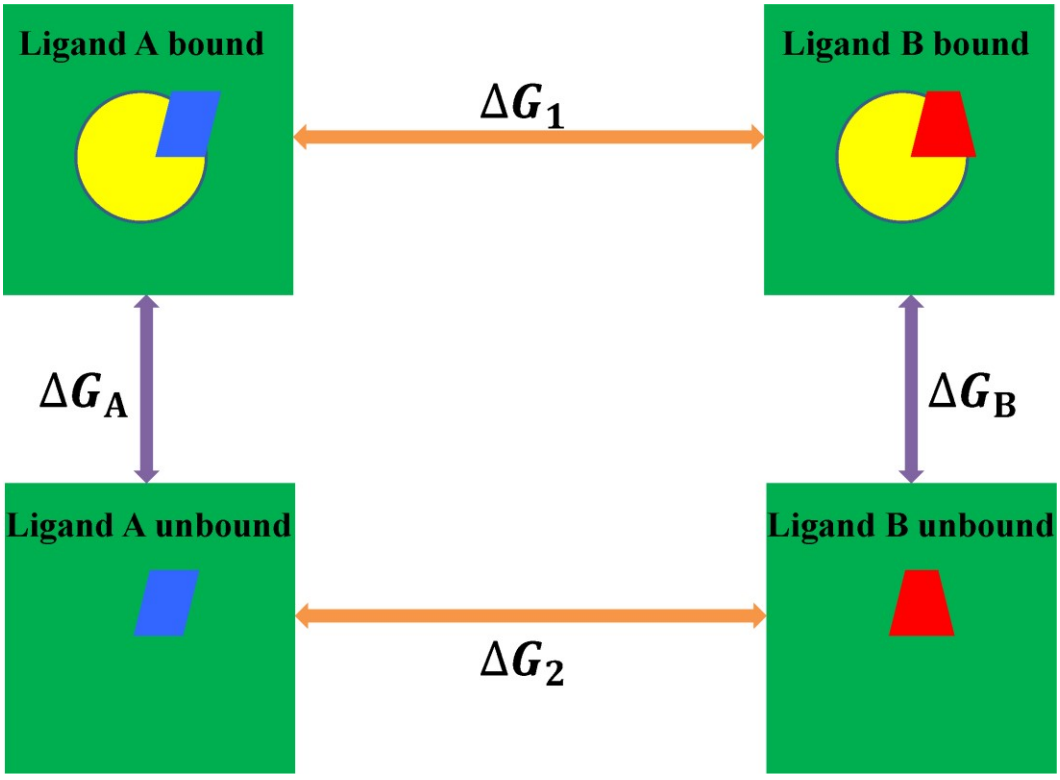

Figure S3. The scheme of relative binding free energy by TI.

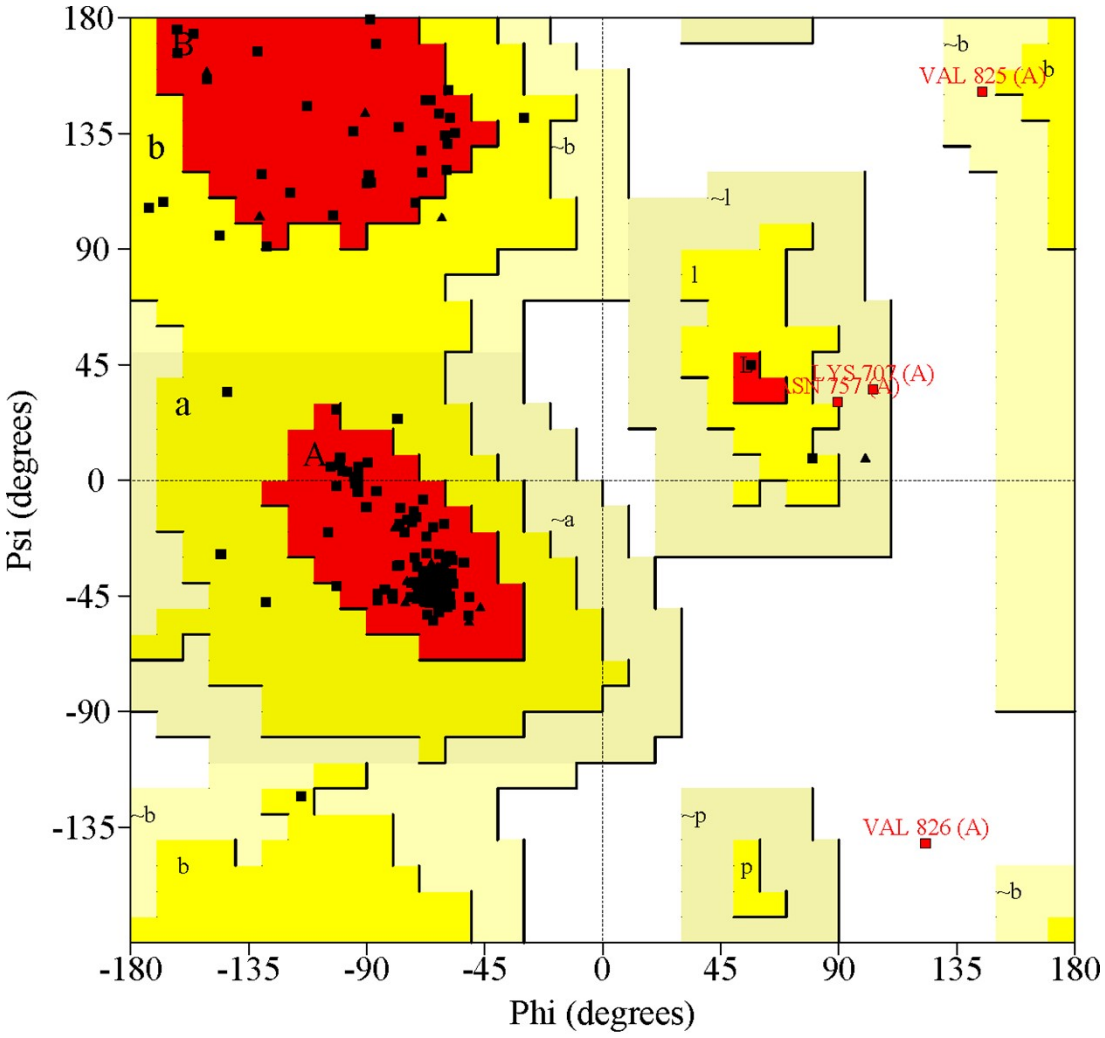

Plot statistics

Residues in most favoured regions [A,B,L]	225	93.8%
Residues in additional allowed regions [a,b,l,p]	11	4.6%
Residues in generously allowed regions [~a,~b,~l,~p]	3	1.2%
Residues in disallowed regions	1	0.4%
Number of non-glycine and non-proline residues	240	100.0%
Number of end-residues (excl. Gly and Pro)	2	
Number of glycine residues (shown as triangles)	19	
Number of proline residues	12	
Total number of residues	273	

Based on an analysis of 118 structures of resolution of at least 2.0 Angstroms and R-factor no greater than 20%, a good quality model would be expected to have over 90% in the most favoured regions.

Figure S4. Ramachandran plot of the homology models for $hmGlu_2$ receptor template as active $hmGlu_5$ atomic coordinates.

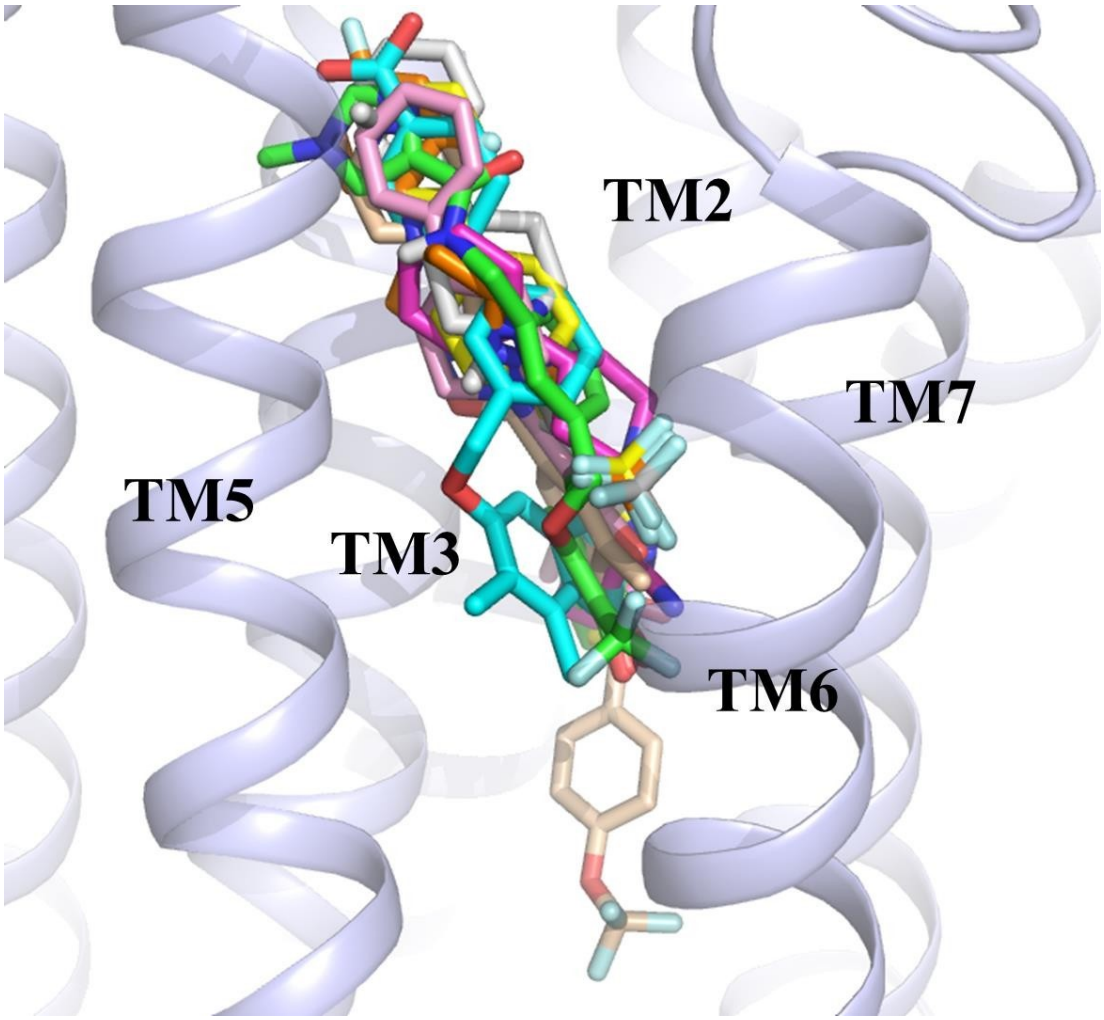

Figure S5. The docking poses of ADX71149 (pink), AZD8529 (brown), BINA (cyan), JNJ40068782 (magenta), JNJ42153605 (yellow), JNJ46281222 (gray), JNJ46356479 (orange), THIIC (green) in allosteric site of $mGlu_2$ receptor (slateblue) shown in ribbon representation.

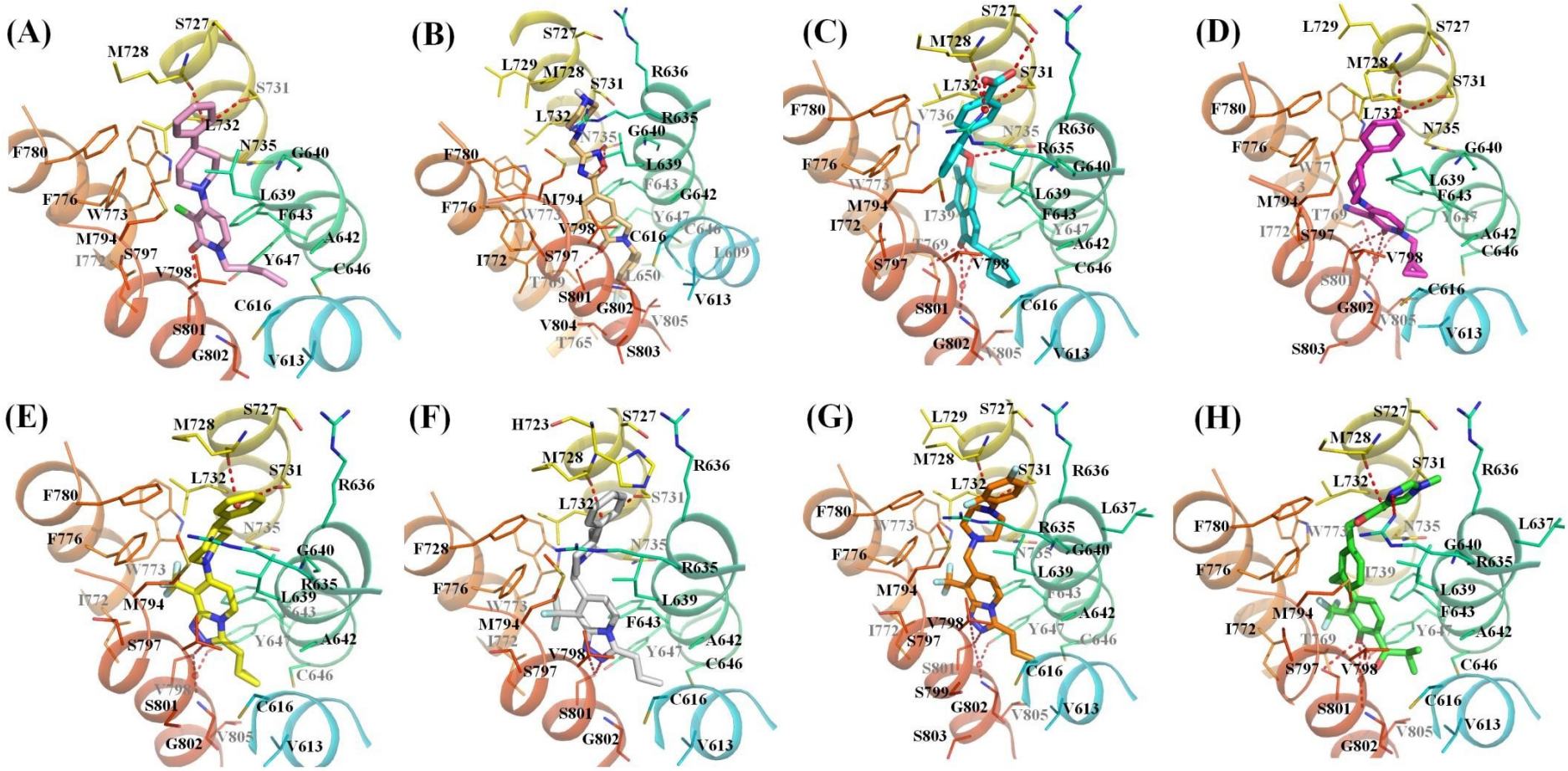

Figure S6. The initial binding poses of 8 studied PAMs in allosteric site of $hmGlu_2$ receptor based on molecular docking. A-H were ADX71149 (pink), AZD8529 (brown), BINA (cyan), JNJ40068782 (magenta), JNJ42153605 (yellow), JNJ46281222 (gray), JNJ46356479 (orange), THIIC (green) shown in stick representation. TM 2, 3, 5, 6 and 7 were displayed in cartoon by yellow, light brown, red, cyan and green respectively. The residues were displayed in line colored as TMs, and were labeled by black and gray color on basis of the location out and in the visual plane respectively. Hydrogen bonds are depicted as red dotted lines and water molecules were displayed as red balls.

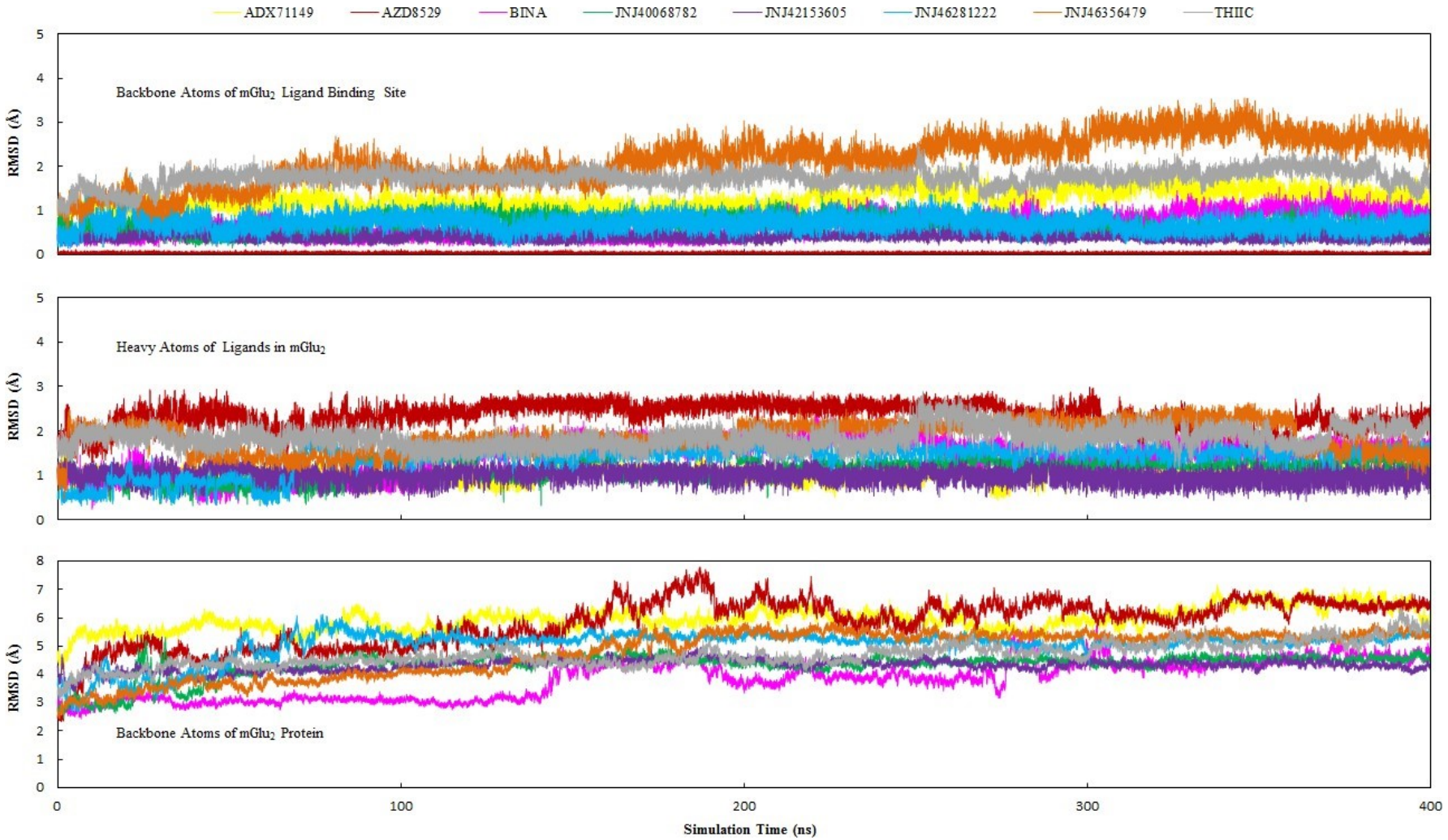

Figure S7. RMSD of protein backbone atoms, ligand heavy atoms and binding site residue atoms as a function of simulation time. All 8 systems reached equilibration state after 50ns with slight fluctuation (within 1Å) in monitored RMSD.

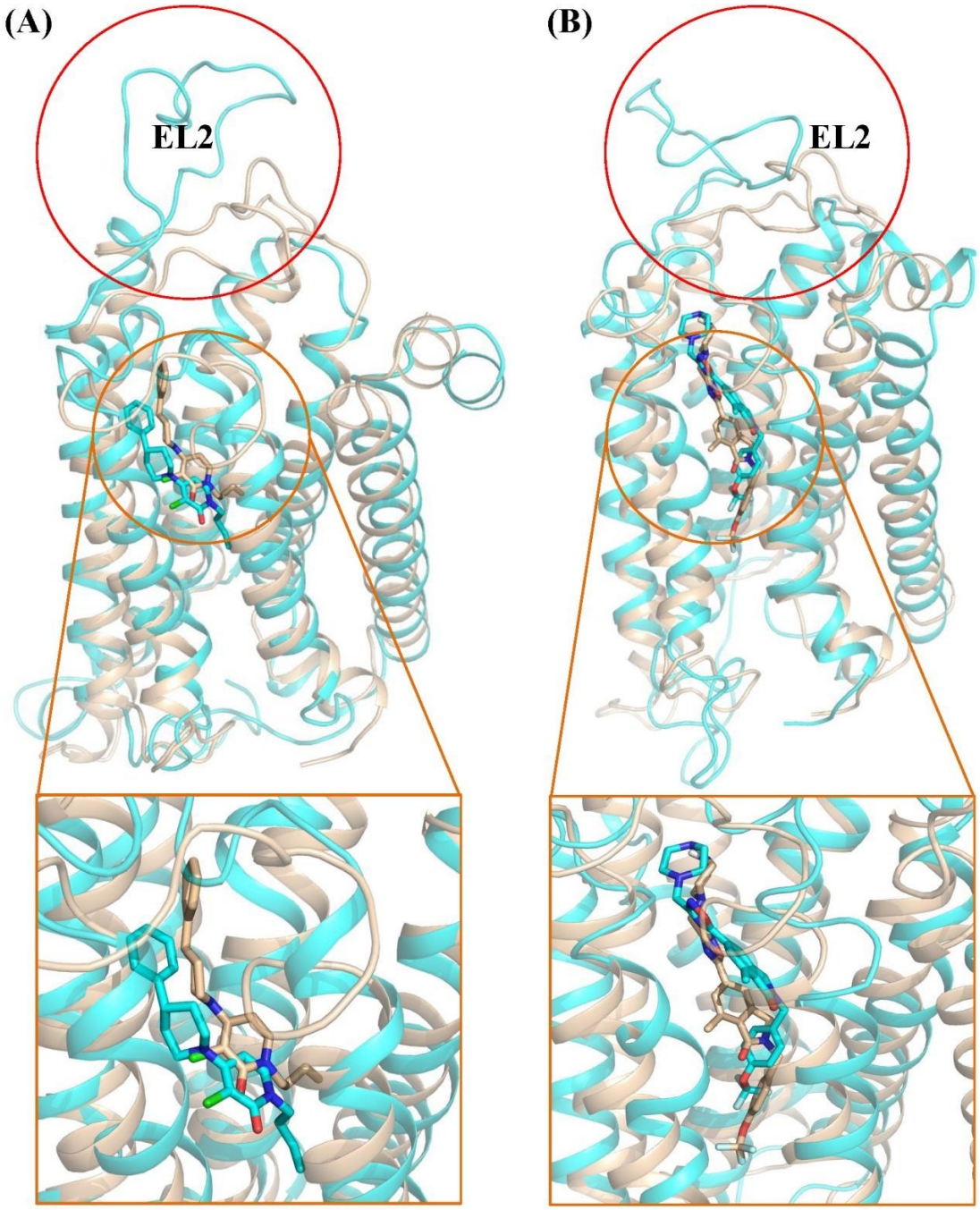

Figure S8. Structural superimposition between initial (light brown) and MD (light blue) structure of ADX71149 (A) and AZD8529 (B).

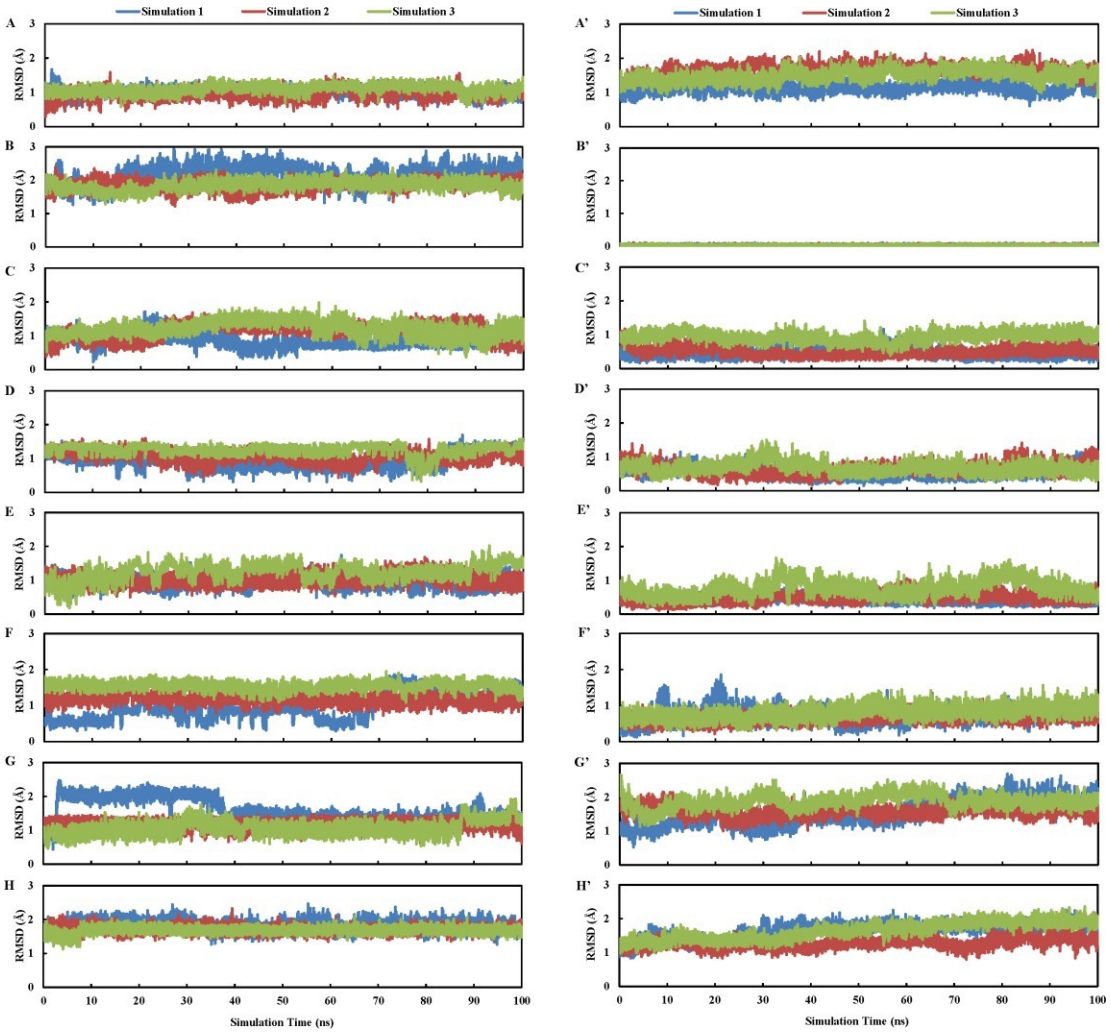

Figure S9. RMSD of ligand heavy atoms and binding site residue atoms for each distinct repetition comparing with the corresponding initial structure during 100 ns simulation. A-H and A-H were RMSD of ligand and binding site for ADX71149, AZD8529, BINA, JNJ40068782, JNJ42153605, JNJ46281222, JNJ46356479, THIIC n $mGlu_2$ receptor respectively.

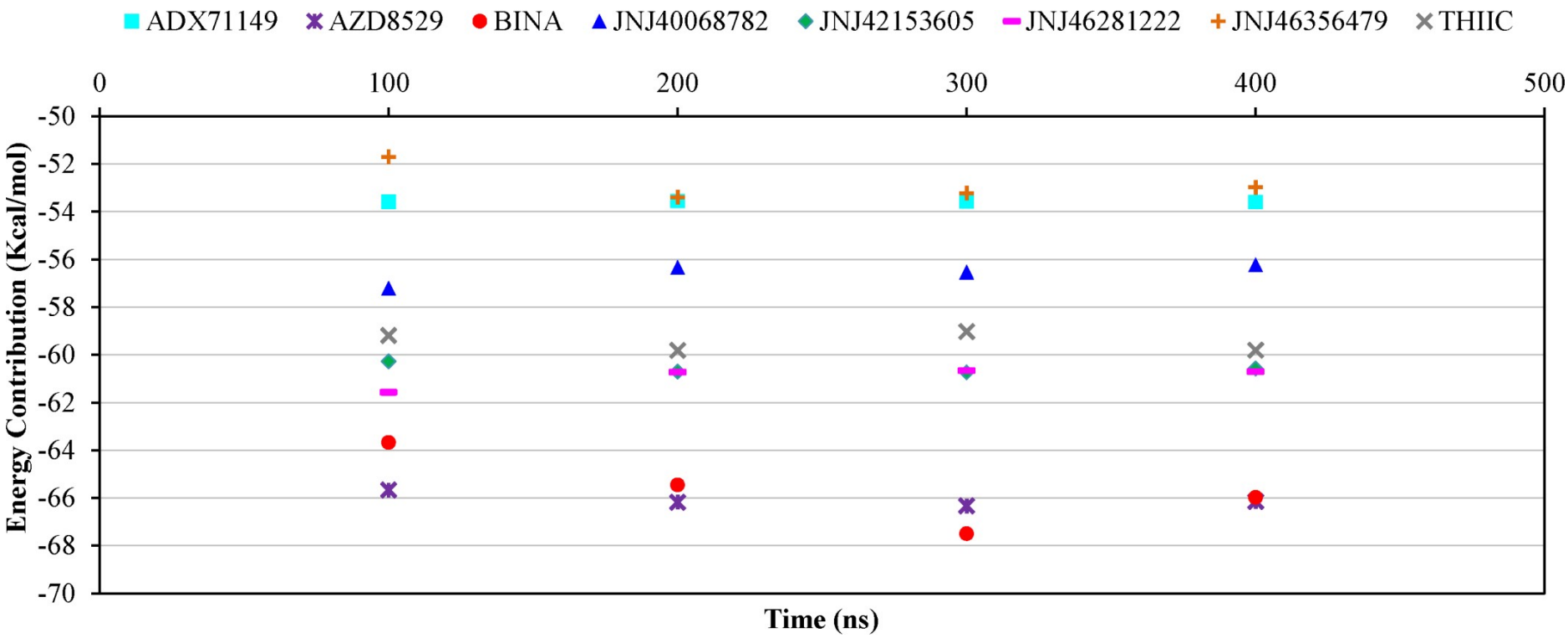

Figure S10. The binding free energies calculated based on 500 snapshots sampled from different simulation windows (50~100 ns, 100~200 ns, 200~300 ns, and 300~400 ns) during the whole 400 ns simulation.

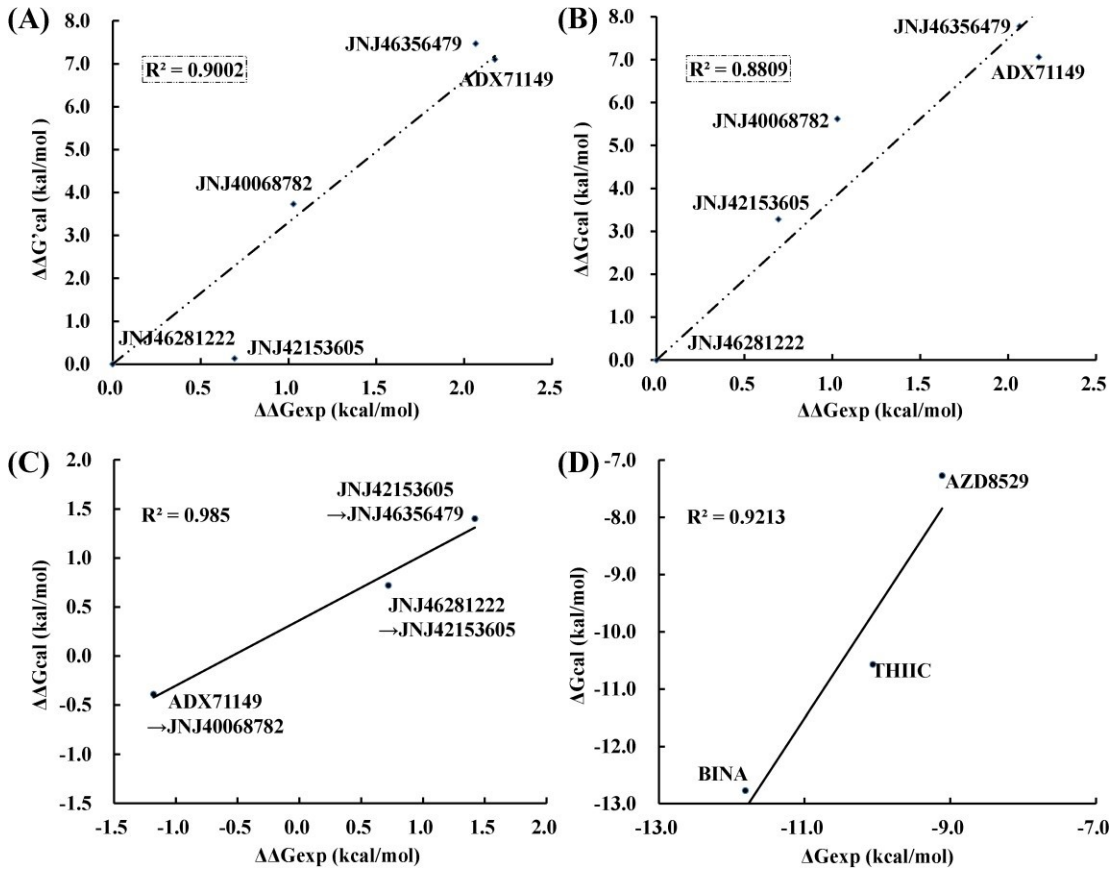

Figure S11. The graphic correlation between experimental and calculated binding free energy. A and B were for ΔΔG′ exclusion of entropy and ΔΔG including entropy in 5 systems with PAMs excepting for three highly dissimilar ligands (AZD8529, BINA, THIIC), C was for relative binding free energy of PAMs with similarity from state A to B in $hmGlu_2$, and D was for absolute binding free energy of 3 ligands with high dissimilarity(AZD8529, BINA, THIIC).

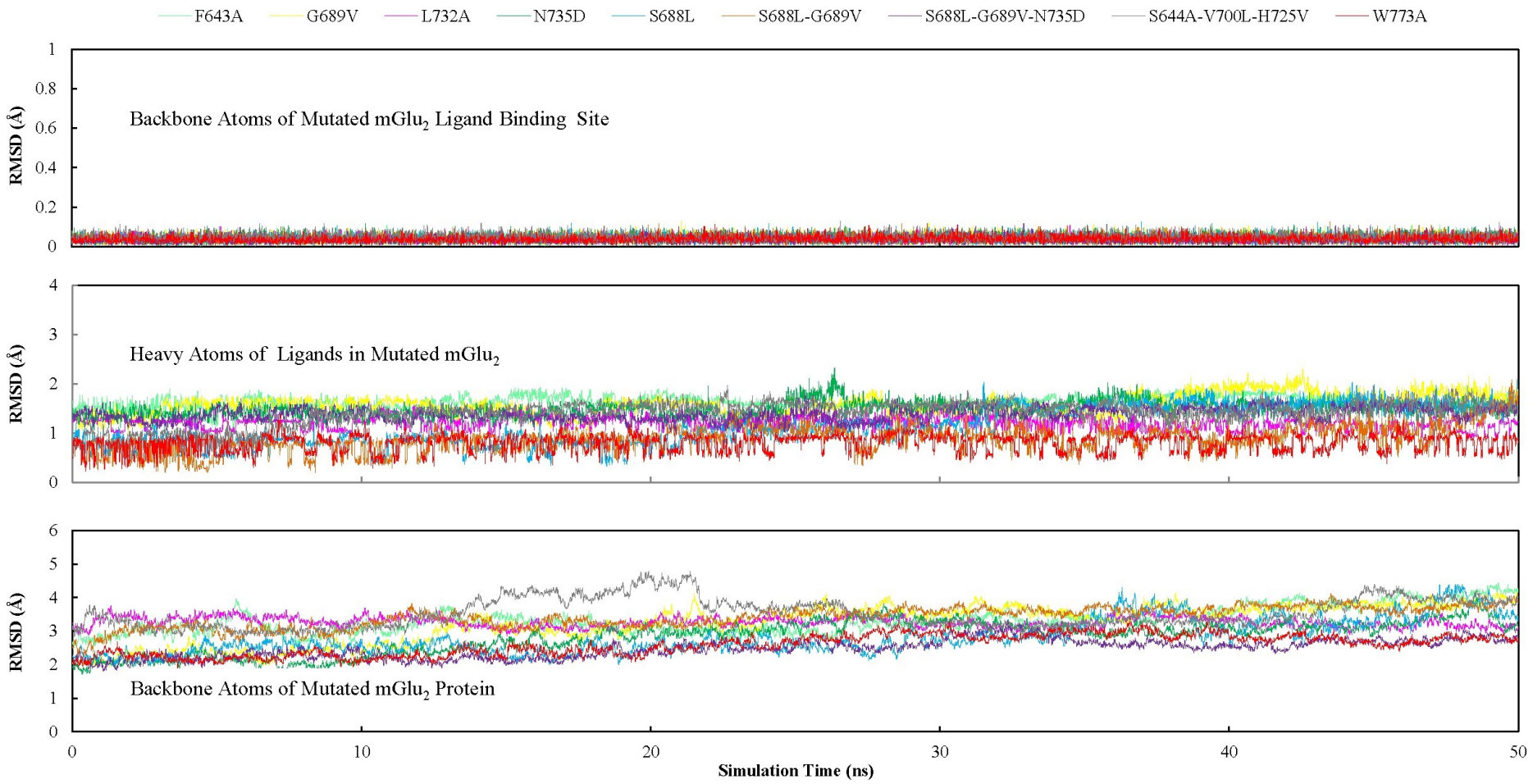

Figure S12. RMSD of protein backbone atoms, ligand heavy atoms and binding site residue atoms for all mutated systems. All 9 mutated systems were studied by adding 50ns simulation based on the MD-simulated wild type $mGlu_2$ receptor.

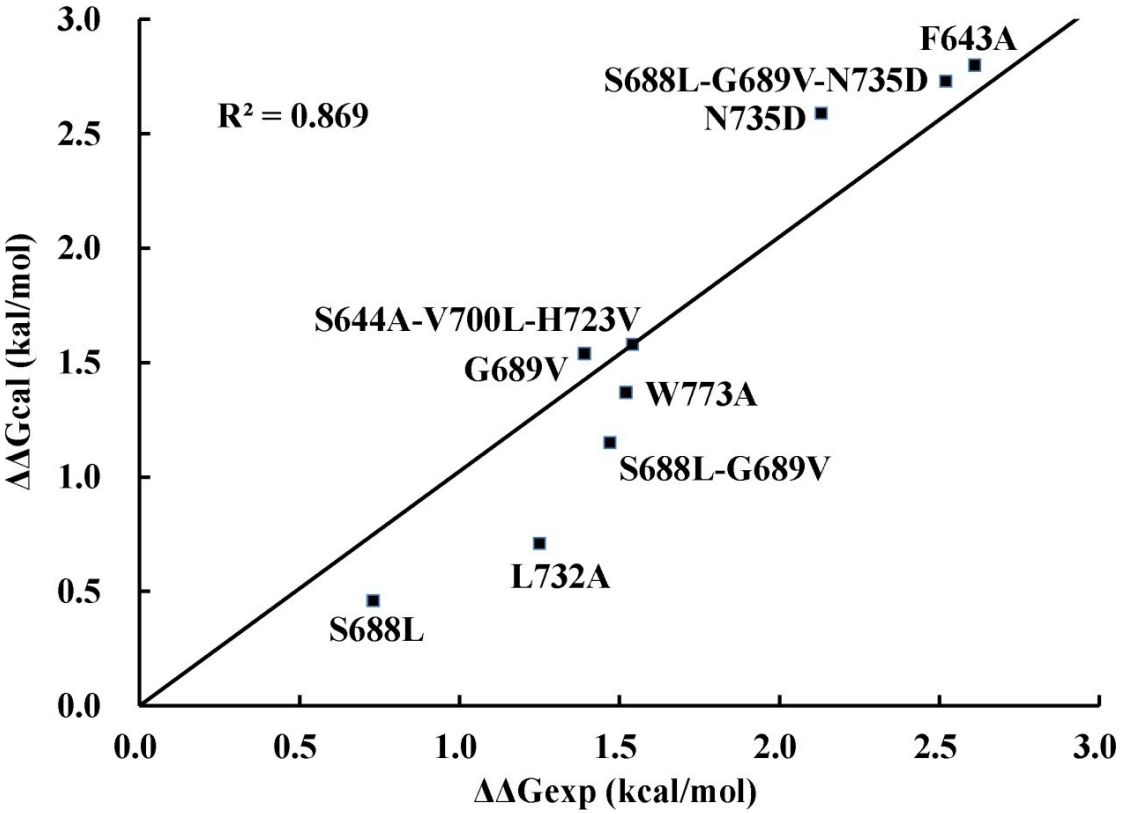

Figure S13. Graphical representation of correlation between the fold changes of simulation ($\Delta\Delta G$) and that of experiment ($\Delta\Delta G_{exp}$) for studied mutant complexes.

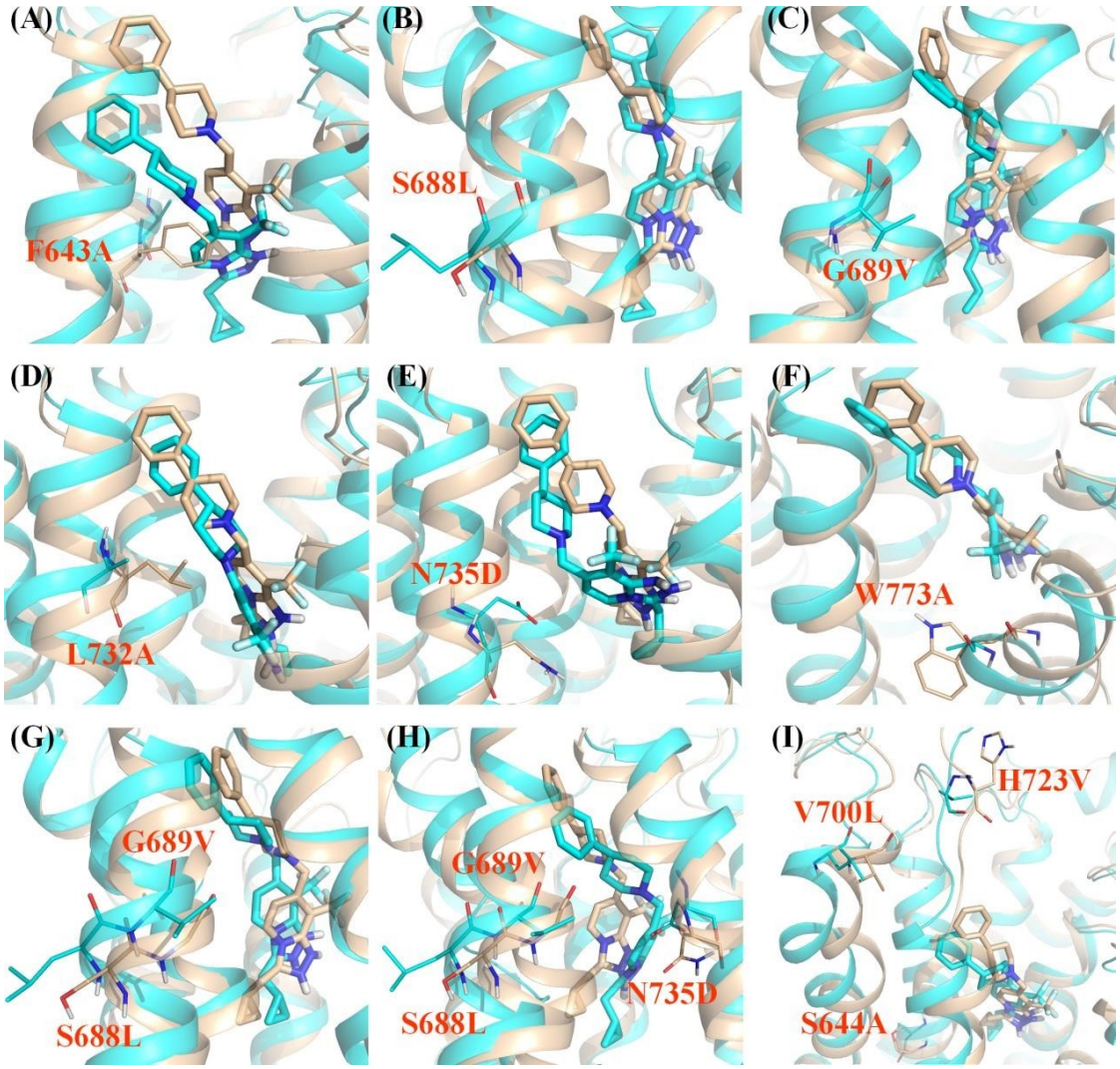

Figure S14. Structural superimposition of (A-I) JNJ46281222 in mGlu2 receptor before and after mutations (F643A, S688L, G689V, L732A, N735D, W773A, S688L-G689V, S688L-G689V-N735D, S644A-V700L-H723V). Mutation residues and JNJ46281222 were shown as a stick representation in wild type (light brown) and mutant (cyan) models.

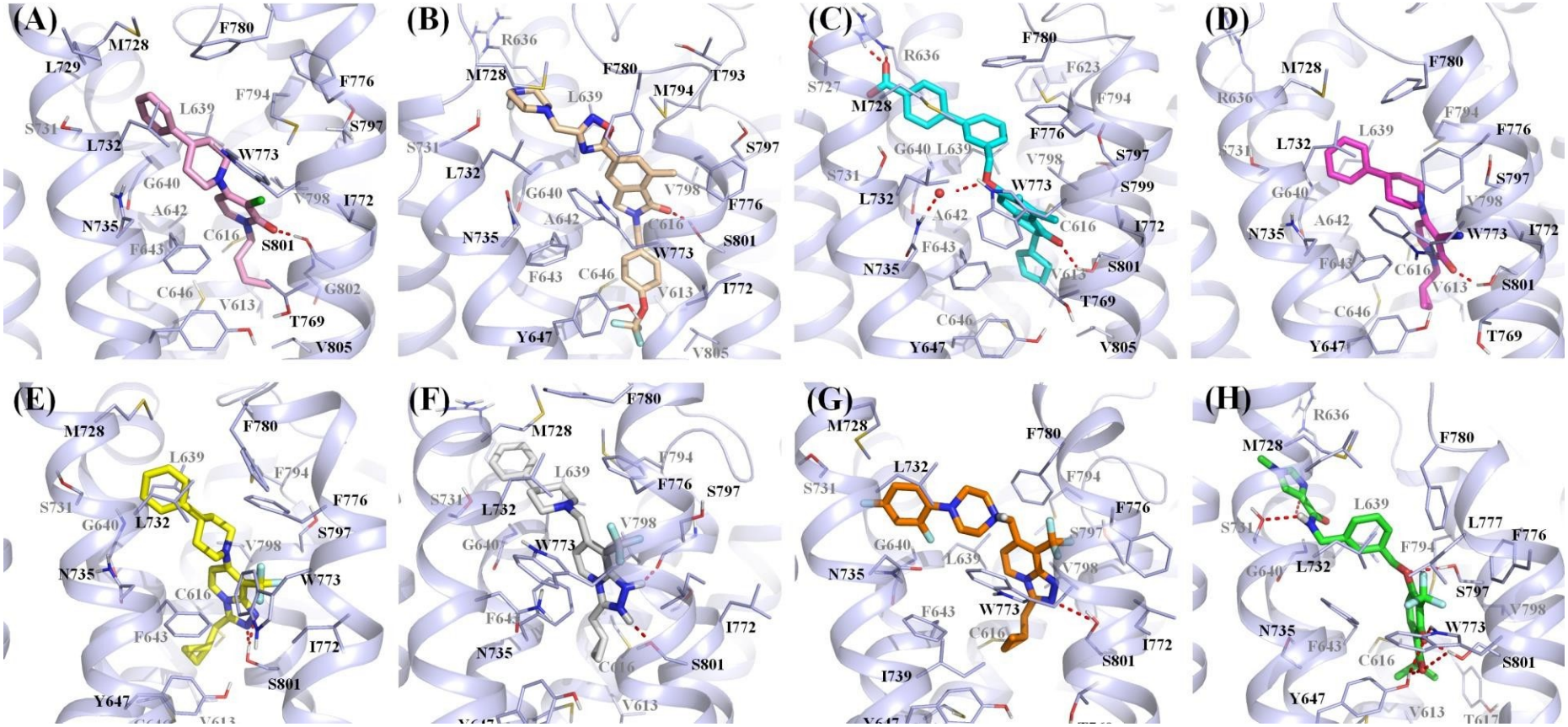

Figure S15. Representative interaction snapshots of 8 studied complexes extracted from equilibrated MD trajectories. A-H were ADX71149 (pink), AZD8529 (brown), BINA (cyan), JNJ40068782 (magenta), JNJ42153605 (yellow), JNJ46281222 (gray), JNJ46356479 (orange), THIIC (green) in $mGlu_2$ receptor respectively. Slateblue cartoon representation was used for the backbone atoms of mGlu2 receptor. Residues and drugs were shown in stick representation, and only polar hydrogen atoms were displayed for clarity. Hydrogen bonds were depicted as red dotted lines and water molecules were displayed as red balls. Residues located out and in the visual plane were illustrated in black and gray color, respectively.

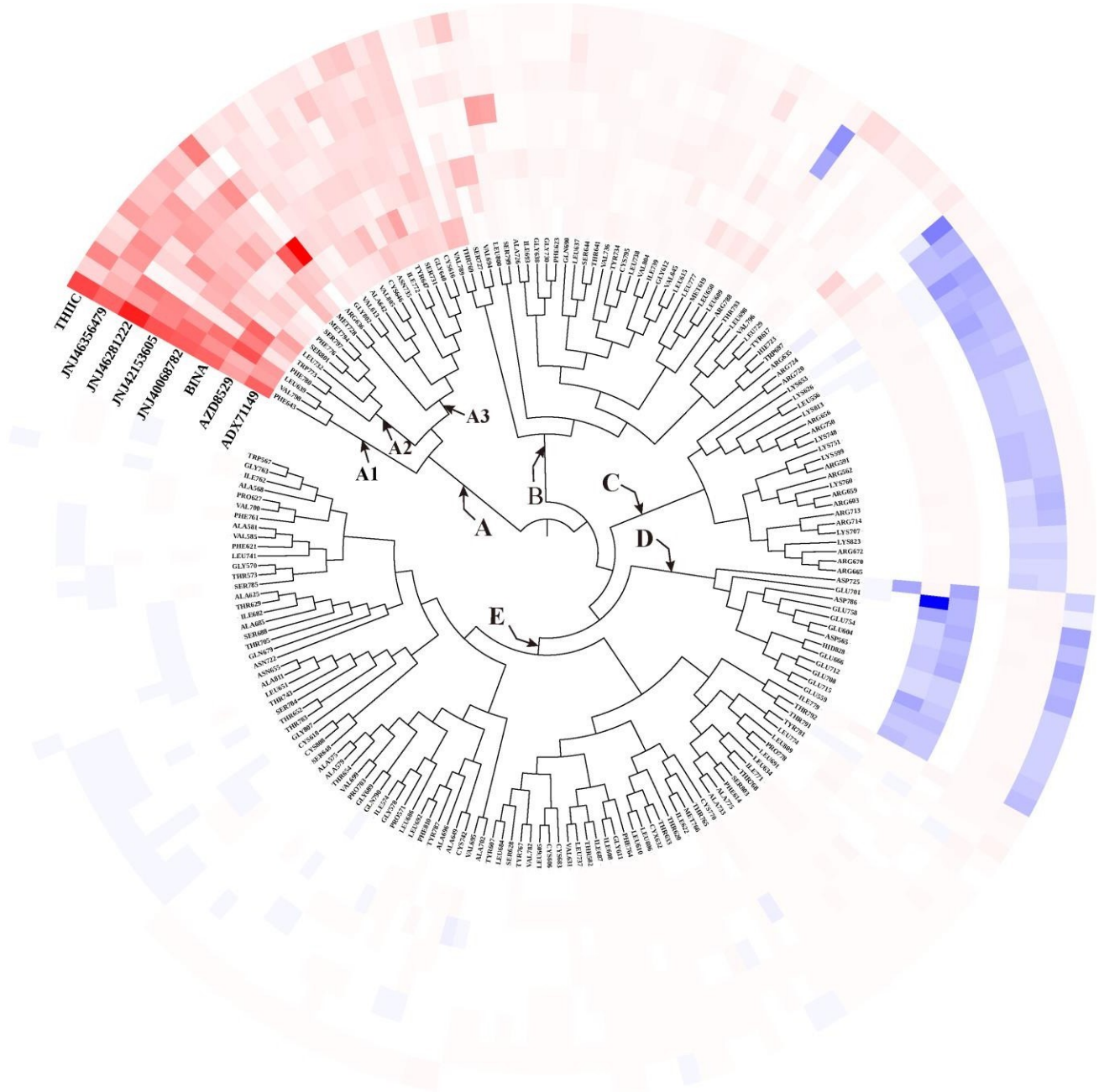

Figure S16. Hierarchical clustering analysis of 186 residues with energy contributions to at least one PAM-hmGlu$_2$ complex based on per-residue binding energy. Per-residue binding energy contributions favoring and hampering binding free energy contributions for PAMs' binding were marked by red and blue, with the standard red and blue for the greatest favoring and hampering respectively. The residues with no affection for ligands' binding were displayed by white, and the lower favoring and hampering contribution gradually fading towards white.

References

1. Perez-Benito, L., Doornbos, M. L. J., Cordomi, A., Peeters, L., Lavreysen, H., Pardo, L.and Tresadern, G. *Structure,* 2017, *25*, 1153-1162 e4.
2. Griebel, G., Pichat, P., Boulay, D., Naimoli, V., Potestio, L., Featherstone, R., Sahni, S., Defex, H., Desvignes, C., Slowinski, F., Vige, X., Bergis, O. E., Sher, R., Kosley, R., Kongsamut, S., Black, M. D.and Varty, G. B. *Sci Rep,* 2016, *6*, 35320.
3. Cid, J. M., Tresadern, G., Vega, J. A., de Lucas, A. I., Del Cerro, A., Matesanz, E., Linares, M. L., Garcia, A., Iturrino, L., Perez-Benito, L., Macdonald, G. J., Oehlrich, D., Lavreysen, H., Peeters, L., Ceusters, M., Ahnaou, A., Drinkenburg, W., Mackie, C., Somers, M.and Trabanco, A. A. *J Med Chem,* 2016, *59*, 8495-507.
4. Doornbos, M. L., Perez-Benito, L., Tresadern, G., Mulder-Krieger, T., Biesmans, I., Trabanco, A. A., Cid, J. M., Lavreysen, H., AP, I. J.and Heitman, L. H. *Br J Pharmacol,* 2016, *173*, 588-600.
5. Farinha, A., Lavreysen, H., Peeters, L., Russo, B., Masure, S., Trabanco, A. A., Cid, J.and Tresadern, G. *Br J Pharmacol,* 2015, *172*, 2383-96.